Synthesis and characterization of lignin hydrogels for potential applications as drug eluting antimicrobial coatings for medical materials

ACS Sustainable Chemistry & Engineering

Article

Synthesis and characterization of lignin hydrogels for potential applications as drug eluting antimicrobial coatings for medical materials.

Eneko Larraneta, Mikel Imizcoz, Jie Xi Toh, Nicola Jayne Irwin, Anastasia Ripolin, Anastasia Perminova, Juan Domínguez-Robles, Alejandro Rodríguez, and Ryan F. Donnelly

ACS Sustainable Chem. Eng., **Just Accepted Manuscript** • DOI: 10.1021/acssuschemeng.8b01371 • Publication Date (Web): 01 Jun 2018

ACS Publications

is published by the American Chemical Society. 1155 Sixteenth Street N.W., Washington, DC 20036

Synthesis and characterization of lignin hydrogels for potential applications as drug eluting antimicrobial coatings for medical materials.

Eneko Larrañeta*, Mikel Imízcoz*, Jie X. Toh*, Nicola J. Irwin*, Anastasia Ripolin*, Anastasia Perminova*, Juan Domínguez-Robles**, Alejandro Rodríguez**, Ryan F. Donnelly*.

The first three authors contributed equally

* Queen's University, Belfast School of Pharmacy, 97 Lisburn Road, Belfast, BT9 7BL, United Kingdom.

** Universidad de Córdoba, Chemical Engineering Department Campus of Rabanales, building Marie Curie, Córdoba, 14071, Spain.

Corresponding author

Dr. Eneko Larrañeta

School of Pharmacy,

Queens University Belfast,

Medical Biology Centre,

97 Lisburn Road,

Belfast

BT9 7BL, UK

Tel: +44 (0)28 9097 2360

Email: **e.larraneta@qub.ac.uk**

Abstract

Lignin is the second most abundant biopolymer on the planet. It is a biocompatible, cheap, environmentally friendly and readily accessible material. It has been reported that these biomacromolecules have antimicrobial activities. Consequently, lignin (LIG) has the potential to be used for biomedical applications. In the present work, a simple method to prepare lignin-based hydrogels is described. The hydrogels were prepared by combining LIG with poly(ethyleneglycol) and poly(methyl vinyl ether-co-maleic acid) through an esterification reaction. The synthesis took place in the solid state and can be accelerated significantly (24h vs 1h) by the use of microwave (MW) radiation. The prepared hydrogels were characterized by evaluation of their swelling capacities and with the use of infrared spectroscopy/solid state nuclear magnetic resonance. The prepared hydrogels showed LIG contents ranging between 40% and 24% and water uptake capabilities up to 500%. Furthermore, the hydrophobic nature of LIG facilitated loading of a model hydrophobic drug (curcumin). The hydrogels were capable of sustaining the delivery of this compound for up to 4 days. Finally, the materials demonstrated logarithmic reductions in adherence of *Staphylococcus aureus* and *Proteus mirabilis* of up to 5.0 relative to the commonly employed medical material poly(vinyl chloride) (PVC).

Keywords: Lignin, hydrogels, drug delivery, antimicrobial materials, solid state reactions, microwave synthesis.

Introduction

The global consumption of fossil fuels is steadily increasing due to industrial development and human population growth. Extensive efforts have been made to find green and sustainable alternatives for material production such as biorenewable polymers[1]. Ligno-cellulose materials have attracted significant attention due to their potential to reduce energy consumption and associated pollution by replacing conventional synthetic materials. This type of material is mainly formed by lignin (LIG), cellulose and hemicellulose[1-6].

LIG is formed from a network of randomly crosslinked hydroxylated and methoxylated phenylpropane units. This molecule is present in the cell walls of cellulosic materials providing mechanical and chemical protection from external stresses. In addition to their mechanical properties, it has been reported that these biomacromolecules have antioxidant and antimicrobial activities[7-10]. Moreover, LIG is the second most abundant renewable biopolymer on the planet[1,11]. However, despite all these factors, LIG technologies remain significantly underdeveloped [1,12]. A minor fraction (less than 2%) of the approximate 70 million tons of LIG produced by the paper industry during the extraction of cellulose is reused for speciality products[1]. The remainder is used as low grade burning fuel or discarded as waste[1,13].

Extensive efforts have been made by the scientific community to develop new types of materials using LIG[1]. LIG has previously been used as a mechanical reinforcement for composites, an antioxidant, a UV protecting agent, an antimicrobial additive, a binder in lithium batteries, as material for water purification and as a biomedical material, amongst other applications[1,11,14-20]. With regards to biomedical applications, hydrogels represent one of the most highly employed materials within this field. Hydrogels are 3D-networks of polymeric chains cross-linked by physical or chemical interactions[21,22]. These materials are similar to biological tissue on account of their high water content and soft consistency[21,22]. LIG-based hydrogels could hold much promise as biomaterials due to the promising characteristics, including the antimicrobial activity, of this biomacromolecule[7,11,23]. Only a few examples have described the use of LIG to prepare hydrogels for biomedical applications. The majority of these studies rely on complex synthetic procedures, involving toxic organic solvents or reagents[1,24], which could ultimately limit applicability of the resulting hydrogels as biomaterials.

In the present work, we propose a facile way to prepare LIG-based hydrogels as potential medical material coatings. The hydrogels are prepared by combining LIG with poly(ethyleneglycol) and poly(methyl vinyl ether-co-maleic acid) through an esterification reaction. The synthesis took place in the solid state and can be accelerated significantly by the use of microwave (MW) radiation. The

hydrogels were characterized and their drug delivery and antimicrobial capabilities evaluated *in vitro*.

Material and methods

Materials

Gantrez® S-97 (GAN) (methylvinylether and maleic acid copolymer) ($Mw = 1.2 \times 10^6$ Da) was provided by Ashland (Tadworth, UK). Poly(ethyleneglycol) (PEG) 10,000 and PEG 400 Daltons were obtained from Sigma-Aldrich (Dorset, UK). Glycerol (GLY) was obtained from VWR (Radnor, USA). LIG was obtained from Tokyo Chemical Industry UK Ltd. (Oxford, UK). CUR was purchased from Cambridge Bioscience (Cambridge, UK). Poly(vinyl chloride) (PVC) sheets (unplasticized, 0.2 mm thickness) were purchased from Goodfellow Ltd. (Cambridge, UK). *Staphylococcus aureus* ATCC 6538 and *Proteus mirabilis* ATCC 35508 (LGC Standards, Middlesex, UK) were maintained on cryopreservative beads (Protect Bacterial Preservation System, Technical Service Consultants Ltd., UK) in 10% glycerol at -80°C. Strains were cultured by inoculation into MHB and incubated at 37°C when required for the *in vitro* microbiological assessments.

Lignin characterization

Lignin was analysed with the purpose of establishing its physicochemical properties. Measurement of the major elements of this sample was carried out on a EuroEA3000 Elemental analyser (EuroVector SpA, Italy) after drying the sample to be analysed (30 mg) overnight at 105ºC.

Acid hydrolysis was performed to determine the Klason lignin and soluble lignin content.[25]. Klason lignin content was determined by gravimetric yield and acid soluble lignin content was determined from the UV-absorption of the hydrolysate at 205 nm[26]. To determine the carbohydrate content, high-performance liquid chromatography (HPLC) analysis was preformed using a previously reported method[27]. Finally, the ash content of the lignin sample was determined gravimetrically by heating the sample to 800ºC and maintaining it at this temperature for 3-6 hours until disappearance of the black carbon particles.

The Fourier Transform Infrared (FTIR) spectrum of the lignin was recorded using a Spectrum Two™ instrument (PerkinElmer, Waltham, MA, USA) equiped with an attenuated total reflectance (ATR) accessory. The spectrum was recorded as an average of 20 scans from 4000 cm^{-1} to 450 cm^{-1} using a resolution of 4 cm^{-1}.

Solid-state ^{13}C nuclear magnetic resonance (NMR) spectra were recorded at 100.63 MHz using a Bruker Avance III HD spectrometer (Bruker, Leiderdorp, The Netherlands) and a 4 mm (rotor o.d.) magic-angle spinning probe. Spectra were obtained using cross-polarisation with TOSS spinning sideband suppression, a 2 sec recycle delay and 1 ms contact time at ambient probe temperature and at a sample spin-rate of 10 kHz. Spectral referencing was performed with respect to an external sample of neat tetramethylsilane (carried out by setting the high-frequency signal from adamantane to 38.5 ppm).

Hydrogel synthesis

Ethanol/water (70% v/v) solutions containing LIG, GAN and PEG/GLY were prepared and 7.5 g of these solutions were cast in 5 x 5 cm moulds. The ethanol/water solutions used in the present work contained 10% (w/w) of LIG, 5% (w/w) of GAN and 5% (w/w) of GLY or PEG. Solutions were allowed to dry over at least 48 h. The resulting films were cut into smaller pieces using a cork borer (diameter 1 cm) and subsequently placed inside an oven at 80°C for 24 h. Subsequently, films were placed in an ethanol/water (70% v/v) solution for 1 week to remove the unreacted reagents. This solution was replaced regularly. Hydrogels were also synthesized using a MW assisted procedure. This procedure is equivalent to the one previously described, but the thermal process (80°C for 24 h) was replaced by a MW assisted process. Samples were placed inside a Panasonic NN-CF778S MW oven (Panasonic UK Ltd, Bracknell, UK) for 1 h at the maximum power setup (1000 W).

Hydrogel characterization

Samples were analysed using an FTIR Accutrac FT/IR-4100 Series (Jasco, Essex, UK) equipped with a MIRacle™ ATR accessory (64 scans and resolution of 4 cm^{-1}). Additionally, a Hitachi TM3030 Scanning electron microscope (SEM) (Tokyo, Japan) was used to evaluate the morphology of the dry and freeze-dried hydrogels.

Solid-state ^{13}C NMR was used to estimate the composition of the hydrogels. The equipment and experimental conditions were as described in section 2.2.

The swelling capabilities of the hydrogels were evaluated by weighing them (m_0), placing them in water and at regular intervals, the films were removed, dried with filter paper to eliminate excess surface water and weighed (m_t). The percentage swelling was calculated by Equation 1.

$$\%\,\text{Swelling} = \frac{m_t - m_o}{m_o} \times 100 \quad (1)$$

The average molecular weight between crosslinks (M_c) was determined using the equilibrium swelling theory. M_c was determined from swelling studies using the Flory and Rehner equation (Equation 3) (2) [28]. All calculations were carried out using the data obtained after swelling the hydrogels in water over a 24 h timeframe.

$$M_c = \frac{-\mathrm{d_p} V_S \phi}{\left(\ln(1-\phi) + \phi + \chi\phi^2\right)} \quad (2)$$

Where: ϕ is the volume fraction of the polymer in the swollen state (equation 3); Vs is the molar volume of water (18 cm^3/mol), and χ is the Flory–Huggins polymer–solvent interaction parameter (equation 4)[29].

$$\phi = \left[1 + \frac{d_p}{d_s}\left(\frac{m_a}{m_b}\right) - \frac{d_p}{d_s}\right]^{-1} \quad (3)$$

$$\chi = \frac{1}{2} + \frac{\phi}{3} \quad (4)$$

In order to calculate ϕ using Equation 3, the following parameters were used: mass of hydrogel before swelling (m_b), mass of hydrogel after swelling (m_a), density of the hydrogel (d_p) and density of the solvent (d_s). The density of the hydrogel films was calculated using Equation 5.

$$d_p = \frac{w}{S \times X} \quad (5)$$

Where *X* is the average thickness of the film, *S* is the cross-sectional area and *w* represents the weight of the film [30].

The crosslink density (V_e) was determined using Equation 6[30,31], where N_A is Avagadro's number (6.023×10^{23} $mole^{-1}$)

$$V_e = \frac{d_p \times N_A}{M_c} \quad (6)$$

Curcumin loading and release

All hydrogels were loaded with CUR by introducing a disc of the respective hydrogel into a glass vial containing 1 ml of CUR-acetone solution (20 mg/ml). After 24 h the disc was dried at room temperature for a duration of ≥24h. To determine total CUR loading, a piece of the disc was transferred into a vial with 20 ml ethanol and after 24 h the released CUR was analysed by UV-VIS spectrometry (PowerWave XS Microplate Spectrophotometer, Bio-Tek, Winooski, USA) at a wavelength of 425 nm. To evaluate drug-polymer interactions, CUR loaded discs were cut in four fragments and analysed using TA Instruments DSC Q100 differential scanning calorimeter (TA Instruments, New Castle, DE, USA). Samples were analysed from 0 to 200°C at a heating rate of 10°C/min.

The release kinetics of CUR loaded discs were studied by introducing a weighed piece of disc into an Eppendorf containing 2 ml of a solution of 90% PBS and 10% Tween 80, to maintain sink conditions, with 0.1% ascorbic acid to prevent CUR degradation. The tubes were placed into an incubator (40 rpm and 37°C). The concentration of CUR was evaluated at defined times using a UV-VIS plate reader at a wavelength of 425 nm and after each measurement the medium was replaced with fresh media. For comparative purposes, the dissolution of pure CUR powder in the release media was evaluated. CUR powder (ca. 1 mg) was placed in a tube containing 16 mL of PBS (pH 7.3) with 10% of Tween 80 and 1 mg/mL of ascorbic acid.

Analysis of release data

The data obtained from the *in vitro* release experiments was fitted to the following mathematical models of drug release: the Korsmeyer-Peppas model (Equation 11), the Higuchi model (Equation 12) and the zero-order kinetic model (Equation 13). In all cases, M_t/M_∞ represents the fractional drug release at time t.

The Korsmeyer-Peppas model exponentially relates drug release with the elapsed time, k_{KP} is the Korsmeyer-Peppas constant, and n is the release exponent indicative of the drug release mechanism[32,33]:

$$\frac{M_t}{M_\infty} = k_{KP} \cdot t^n \quad (11)$$

The Higuchi model (Equation 12) is used mainly for situations where Fickian diffusion governs the release process[33]. k_H is the Higuchi constant.

$$\frac{M_t}{M_\infty} = \mathrm{k}_H \cdot \mathrm{t}^{0.5} \quad (12)$$

The zero-order kinetics equation (Equation 13) is used when the system releases the same amount of drug per unit of time [33]. In this case k_{ZO} is the zero order constant.

$$\frac{M_t}{M_\infty} = \mathrm{k}_{\mathrm{ZO}} \cdot \mathrm{t} \quad (13)$$

In vitro microbiological assessment

A GAN hydrogel containing no lignin (GANPEG) was prepared as one of the controls for the *in vitro* microbiological assessments, following the previously described procedure. For this purpose, an aqueous blend containing 20% (w/w) GAN and 7.5% (w/w) PEG was used. This hydrogel has been used and described extensively for drug delivery purposes[30,34,35]. Bacterial suspensions (1 x 10^6 cfumL^{-1}) of *P. mirabilis* and *S. aureus* were prepared as described in one of our previous works[36]. Hydrogel films and PVC controls (10 x 10 mm) were immersed in the bacterial suspensions (1 mL) within individual wells of a tissue culture plate. The materials had previously been soaking in deionized water for 0h, 24h and 7 days. Samples were shaken at 100 rpm in an orbital incubator at 37°C. Following 4 h and 24 h incubation periods, samples were removed from the bacterial suspension, rinsed and sonicated in QSRS as described in our previous work[36]. Viable counts of the resulting QSRS were performed by the Miles and Misra serial dilution technique[37], with plating onto low-swarm (LSW) agar (*P. mirabilis*) or Mueller-Hinton agar (*S. aureus)* to determine the number of adherent bacteria on each sample surface. Numbers of adherent bacteria after 4 h and 24 h incubation are expressed as percentage values relative to PVC controls.

Statistical analysis

All data were expressed as mean ± standard deviation. Data were compared using a One-Way Analysis of Variance (ANOVA), with Tukey's HSD post-hoc test for more than two means. In all cases, $p < 0.05$ was the minimum value considered acceptable for rejection of the null hypothesis.

Results and discussion

Lignin characterization

LIG from a commercial source was selected for this work. Details of the major characteristics of the material, such as composition or origin, were, however, not provided. The complete LIG characterization can be found in the supporting information. Analysis of the LIG sample showed that ~80% of the product was LIG (Table S1) and that there was a significant amount of inorganic particles (ca. 15%). Consequently, this reinforced the need to wash the hydrogels after synthesis to remove all impurities. Finally, the sample did not show any presence of cellulose contamination. The results obtained for the chemical composition and the FTIR and NMR analysis of the LIG samples (Figures S1 and S2) suggest that the lignin was isolated from wood using a pulping process containing sulphur delignifying agents and/or was precipitated using sulphuric acid.

Lignin-based hydrogels synthesis and characterization

LIG hydrogels were synthesized for potential biomedical applications by using GAN as a crosslinker. GAN/PEG hydrogels have been extensively studied for drug release applications[34,38,39]. These hydrogels are based on the esterification of the GAN acid groups with the OH groups present in PEG molecules[34,38,39]. LIG contains a large amount of alcohol groups therefore represents an ideal candidate to be crosslinked with GAN. Additionally, GAN and LIG have been shown to be biocompatible and non-toxic[40,41]. Hydrogels were firstly prepared with GAN and LIG. However, the resulting films presented several limitations. The obtained films were not flat and were too brittle to handle in their dry state, therefore could not be used. It has been reported previously that GAN films are brittle in nature and they require a plasticizer to be used for drug delivery applications[42]. Additionally, after swelling, the materials disintegrated upon removal from the PBS solution as a result of their low crosslinking density and the swelling capacity of the hydrogels could therefore not be measured. The LIG employed presented a high molecular weight (ca. 60 kDa)[43,44] and, consequently, the resulting hydrogels presented an expanded structure that could accommodate large amounts of water. Consequently, a third component was added to provide a higher crosslinking degree and to act as a plasticizer of the films. PEG molecules seemed to be a good candidate for this purpose as they have been used previously as a GAN crosslinker[34,38,39]. Moreover, Shing *et al.* reported that PEG is a good plasticizer for GAN films[42]. Therefore, in the present study, PEG molecules with different molecular weights were used as plasticizer/crosslinker to ascertain the effect of the PEG type on the properties of the final hydrogel (Table 1). In addition, GLY was used in order to evaluate the effect of a smaller molecule as a potential plasticizer/crosslinker (Table 1).

Table 1. Composition and calculated network parameters for the LIG-based hydrogels.

Hydrogel	Mw PEG	Weight ratio*		Composition (%) (w/w)*			Network Parameters			
		LIG/GAN	LIG/PEG	LIG	GAN	PEG	φ	M_c (Equi) (kDa)	χ	V_e x 10^{-19}
LIG14K	14,000	1.5	1.3	41.1	27.4	31.6	0.15	70.0	0.55	0.96
LIG10K	10,000	1.4	1.1	38.1	27.2	34.7	0.17	40.9	0.56	1.59
LIG400	400	0.9	0.5	24.3	27.0	48.6	0.21	18.4	0.57	3.59
LIGGLY	-**	0.5	-	-	-	-	0.17	46.5	0.56	1.54

* Calculated using solid state ^{13}C-NMR measurements

** LIGGLY hydrogels contain GLY instead of PEG

Figure 1 shows the chemical structures of LIG, GAN and PEG, and the proposed crosslinking reaction for the LIG/GAN/PEG hydrogels. It has previously been reported that GAN can be crosslinked with PEG *via* an esterification reaction [30,34,38,39]. Consequently, it was expected that a molecule with multiple OH group such as LIG would be facilely added to the structure (Figure 1). A similar behaviour was expected when combining GAN, LIG and GLY since the GLY molecule contains three OH groups.

The esterification reaction takes place in the solid phase. Therefore, we can hypothesize that before the crosslinking reaction some of the OH groups present in PEG/LIG are aligned with the COOH groups present in GAN chains, forming hydrogen bonds, as previously proposed by Singh *et al*[42]. During the crosslinking process the supplied thermal energy allows the formation of ester bonds between the previously aligned COOH and OH groups.

To ascertain the crosslinking chemical reaction, FTIR spectroscopy was used. Representative spectra of the pure compounds and non-crosslinked and crosslinked hydrogels can be found in the supporting information (Figure S3). The main changes are within the carbonyl region. GAN carboxylic acids react with alcohol groups in LIG and PEG to form ester bonds. Figure 1B shows the FTIR spectra of the carbonyl region for the hydrogels before and after the crosslinking reaction. It is noticeable that the carbonyl peak shows a displacement to higher wavenumbers after the crosslinking process. The infrared carbonyl peaks for the carboxylic acids and esters are overlapping

and the peak shift suggests the presence of a new ester peak which overlaps with the previous acid peak[36,45].

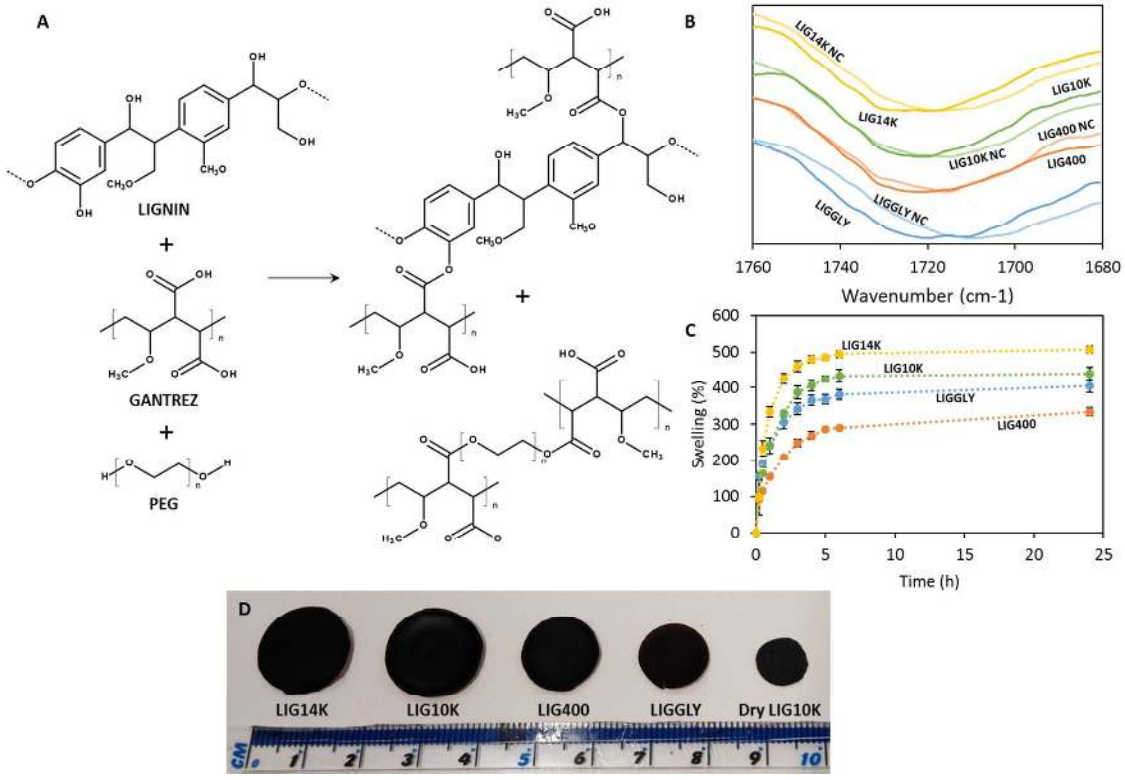

Figure 1. Chemical structure of LIG, GAN and PEG and proposed crosslinking reactions (A). FTIR spectra of the carbonyl region of of LIG/GAN/PEG hydrogels before (NC) and after the crosslinking process (B). Swelling kinetics of LIG-based hydrogels in PBS (C). Images of all swollen LIG-based hydrogels and the unhydrated LIG10K (n=3) (D).

To determine the amount of GAN, PEG and LIG in the hydrogels, solid state ^{13}C NMR was used. Table 1 shows the composition of the hydrogels measured using solid state 13C-NMR (see supporting information Figure S4). The composition of the LIGGLY hydrogel could not be estimated due to the low intensity and overlap of the peak assigned to GLY at 77-66 ppm with peaks from GAN and LIG. On the other hand, the obtained results for the remaining hydrogels showed that the amount of GAN remained almost unaltered for all hydrogels at approximately 27% (w/w). LIG14K and LIG10K showed similar compositions, with a LIG percentage of ~40% (w/w) and a PEG concentration of ~32% (w/w). LIG400 showed a lower LIG concentration, ~25% (w/w), and a higher PEG concentration. As described before, the composition of LIGGLY hydrogels could not be fully analysed

as the GLY peak is so small that it is overlapping with the LIG peaks. Consequently, the GLY concentration could not be properly calculated but we can assume that it is significantly lower than the PEG composition in the previous hydrogels. Moreover, it can be seen that the 13C-NMR spectrum of LIGGLY showed smaller LIG associated peaks (158-100 ppm) than the rest of the hydrogels. By comparing the peaks at 185-165 ppm and 158-100 ppm it can be estimated that LIGGLY presented the lowest LIG/GAN weight ratio (0.5).

The results showed that the GAN concentration remained almost constant and the LIG concentration decreased while the PEG concentration increased. This suggests that the molecular weight of the second crosslinker significantly influenced the ability of LIG to bind to the GAN structure. It can be hypothesized that when GAN was crosslinked with the higher molecular weight PEG, the network had more space to accommodate LIG molecules within the structure. On the other hand, when smaller crosslinkers were used, the network presented a more compact structure that prevented ready accommodation of LIG within the structure. It is important to note that when using GLY as a crosslinker the effect is slightly different. We obtained hydrogels with a lower LIG content and a low GLY content that could not be properly determined. This suggest that LIG prevents the reaction of GAN with GLY. Therefore, the resulting hydrogels are formed mainly by GAN and LIG.

In order to gain more understanding about the hydrogel structure and the corresponding behaviour when placed in contact with an aqueous environment, the swelling kinetics of the materials in PBS were studied. Figure 1C shows the swelling curves as a function of time for all synthesized hydrogels. It can be seen that all hydrogels showed similar swelling profiles, reaching the maximum water uptake after approximately five hours. All hydrogels presented different maximum water uptakes ($p < 0.05$). LIG14K showed the highest degree of swelling, followed by LIG10K. This was expected since the composition of both hydrogels was similar but LIG14K had a longer crosslinker (PEG 14,000 vs PEG 10,000). The only two hydrogels that showed no significant difference in their maximum water uptakes were LIGGLY and LIG10K ($p = 0.215$). Interestingly, LIG400 showed a lower swelling capacity than LIGGLY. LIG400 showed a high amount of PEG 400 in the hydrogel (Table 1) suggesting that this linear polymer was the main crosslinker limiting incorporation of LIG in the structure. Additionally, table 1 showed that these hydrogels presented the lowest LIG/GAN ratios. As explained previously, the NMR analysis suggested that LIGGLY hydrogels were formed mainly from GAN and LIG. These hydrogels contained a small amount of GLY and consequently the crosslinking of GAN with LIG molecules will lead to a more loosely crosslinked structure and higher swelling degrees than LIG400 that contains LIG and PEG400 as crosslinkers. This hypothesis would explain why LIGGLY did not present the lowest degree of swelling. Moreover, Figure 1D shows representative images of the swollen hydrogels. For comparative purposes, a sample of unhydrated LIG10K was included in the

images. Interestingly, LIGGLY hydrogels appeared smaller in size than the LIG400 hydrogels despite having a higher swelling capacity. As can be seen in Table 1, LIGGLY presented the lowest LIG/GAN ratio. A high amount of the initial LIG did not react with GAN chains and, consequently, was washed away after synthesis. Therefore, LIGGLY hydrogels are significantly smaller after washing. GAN-based hydrogels have previously been prepared using different types of crosslinkers such as poly(vinylalcohol), GLY, PEG or poloxamers[46-51]. However, the majority of these hydrogels showed higher swelling degrees as they only used one crosslinker.

Table 1 shows the calculated network parameters for all synthesized hydrogels. As expected, the average molecular weight between crosslinks increased with the swelling capacity of the hydrogels. The volume fraction of polymer in the swollen state (ϕ) is described as a ratio of the polymer volume to the swollen gel volume (Equation 3)[30]. As can be seen in Table 1, the hydrogels with higher swelling capacity showed higher ϕ values. The higher the value of χ, the weaker was the interaction between the polymer and water. Therefore, increasing the crosslinking degree increased the interaction between the polymeric system and water. Finally, V_e represents the number of elastically effective chains, totally induced in a perfect network, per unit volume[30,31]. Consequently, hydrogels with higher crosslinking densities presented higher values of V_e. The calculated V_e values were consistent with the results obtained in the swelling studies.

Figure 2 shows SEM images of the hydrogels after swelling/freeze drying. The SEM images of the hydrogels before swelling can be seen in the supporting information (Figure S5). It can be seen that all the dry hydrogels showed a certain degree of porosity that can be attributed to LIG. The only exception was LIGGLY, which showed a highly compact structure. From analysis of the NMR results it was obvious that these hydrogels were mainly formed by GAN and LIG, presenting a lower LIG/GAN ratio (0.5). Consequently, the lower LIG content would explain the compact structure. Additionally, the freeze dried hydrogels showed bigger pores (see supporting information Figure S5). The pore sizes could be correlated with the maximum water uptake. LIG14K, LIG10K and LIGGLY showed larger holes and pores in their structure after removal of the water, while LIG400 showed a more uniform and smaller pore size distribution. This was a direct consequence of its lower water uptake.

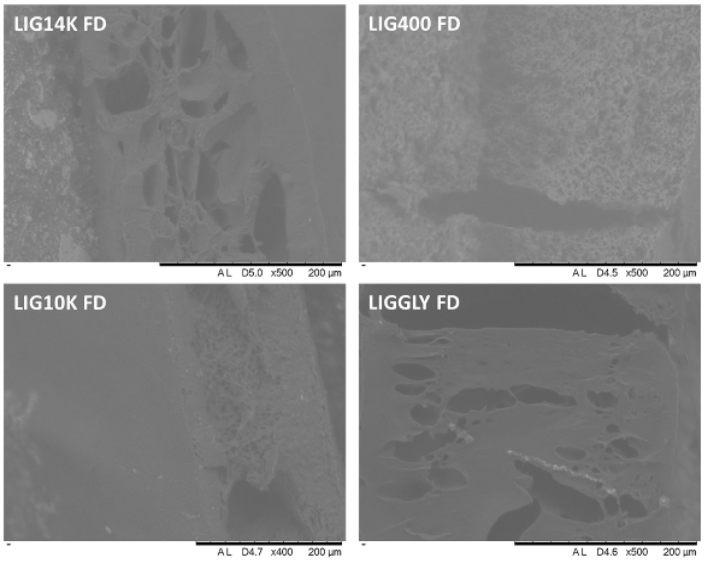

Figure 2. SEM images of freeze dried (FD) hydrogels.

All results shown in this section support the use of the process developed herein for the preparation of LIG-based hydrogels. The synthetic process does not require the use of any toxic solvents or reagents. The solvent employed was an ethanol/water mixture, and it has been previously reported that methanol/water or ethanol/water mixtures are environmentally favourable compared to other types of organic solvents such as pure alcohol or propanol/water mixtures[52]. Furthermore, the crosslinking reaction is an esterification process and the main by-product of these reactions is water. Consequently, it can be established that the process is a green process as the used reagents did not present any danger or toxicity for the environment and no toxic side-products were generated.

Curcumin loading and release from the lignin-based hydrogels

Several authors have reported the inclusion of hydrophobic moieties within hydrogel structures as a mechanism of improving hydrophobic drug loading[53]. Consequently, LIG-based hydrogels have potential to be used as hydrophobic drug delivery systems. CUR was selected as a model hydrophobic compound to evaluate the capability of LIG-containing hydrogels to load and release hydrophobic drugs. Figure 3A shows the obtained CUR loading for all the LIG-containing hydrogels. It can be seen that the hydrogels with higher LIG content presented higher CUR loading and the loading can be correlated with the LIG/GAN weight ratio of the hydrogels. LIG is a molecule rich in aromatic rings and CUR contains two aromatic rings. Consequently, the interaction between aromatic rings could explain this trend. The interaction between CUR molecules and other aromatic

ring-containing molecules has been extensively described in the literature[54]. All the hydrogels presented different degrees of CUR loading ($p < 0.05$). However, there were no significant differences between LIG14K and LIG10K loadings ($p = 0.091$). This hypothesis can be confirmed through DSC measurements (Figure 3B). The CUR DSC curve showed a sharp endothermic melting point at around 180°C. This peak cannot be observed in the hydrogels loaded with CUR suggesting that cargo molecules are interacting with the hydrogel structure and consequently they are not forming crystals. In the literature, similar results can be found for other types of CUR supramolecular complexes such as CUR/cyclodextrin complexes[55].

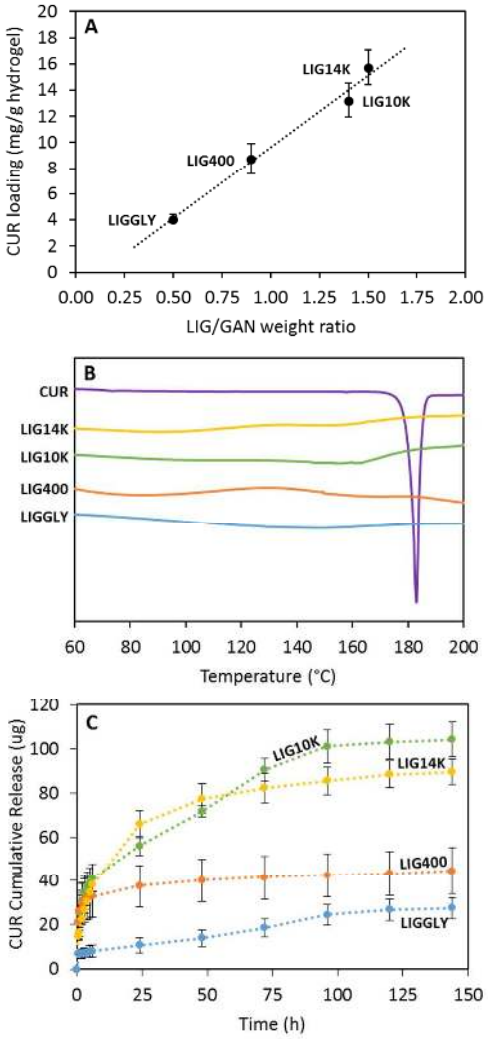

Figure 3. Correlation between the CUR loading and the LIG/GAN weight ratio in the hydrogels (n=3) (A). DSC curves for CUR and CUR loaded hydrogels (B). For all thermograms: Exo Up. CUR cumulative release from all the hydrogels (C). (n=3).

Figure 3C and Figure S6 (Supporting information) show CUR cumulative release from all synthesized hydrogels. It can be seen that LIG14K and LIG10K released the largest amount of CUR, followed by LIG400 and then LIGGLY. This was consistent with the loading results. Moreover, it can be seen that LIG400 did not show a sustained release since the hydrogels released all their CUR cargo within a few hours. The other hydrogels showed CUR release over several days, and up to four days for LIG10K and LIGGLY. The latter showed promising capabilities for sustaining the release, however, it is not an ideal candidate due to the poor CUR loading. The optimal hydrogels in terms of CUR loading and release were LIG14K and LIG10K. LIG10K showed a linear release profile after an initial burst release of the cargo. On the other hand, LIG14K hydrogels did not show this biphasic pattern in their release profiles. Both hydrogels contained similar LIG concentrations. Consequently, it seems that as LIG10K showed a lower water uptake capacity (Figure 1C) it presented a more compact structure and a slower diffusion of CUR from the hydrogel matrix. The solubility of CUR was not the main factor behind the sustained release of CUR from the hydrogels as the dissolution of equivalent amounts of pure CUR powder was complete within 3-4 hours (data not shown).

In order to ascertain the release mechanism of CUR from the hydrogels, different mathematical models were used. Table S3 (supporting information) shows calculated parameters obtained after fitting the release data to the equations described in the material and methods section. The results showed that the only hydrogel showing a diffusion-based release mechanism was LIG14K, with *n* value close to 0.45 for the Korsmeyer-Peppas model and good fitting to the Higuchi model (Fickian diffusion model). On the other hand, LIGGLY and LIG10K presented linear release after the initial burst release. Their lineal section showed good fit to the Zero-Order model (see supporting information Table S3). This can be explained by the similar swelling profile of both hydrogels. However, LIGGLY presented poor CUR loading capabilities. Overall, after evaluating the composition and behaviour of the hydrogels and by evaluating the CUR release kinetics, we can conclude that LIG10K showed the most promising capabilities for biomedical applications (high lignin content, high CUR loading while providing sustained release). Consequently, LIG10K was used in the following studies to evaluate the antimicrobial properties of LIG-based hydrogels.

In vitro microbiological assessment

Nosocomial infections primarily result from bacterial attachment to surfaces, for example of implanted medical devices, and resulting biofilm formation[56]. These infections demonstrate significant resistance to antibacterial treatment, resulting in extended hospital stays, increased healthcare costs, patient morbidity and potential mortality [57]. Consequently, antimicrobial

materials/coatings have attracted the attention of researchers during recent years[58,59]. Due to the antimicrobial properties of LIG, the LIG10K hydrogels were evaluated as potential antimicrobial coatings for medical devices. The LIG10K hydrogel and a control hydrogel (GANPEG) (without LIG) were herein tested for their *in vitro* resistance to adherence of the Gram-positive pathogen, *Staphylococcus aureus* (Figure 4ia), a common causative agent of nosocomial bloodstream and medical device-associated infections[60] and the Gram-negative urinary pathogen, *Proteus mirabilis* (Figure 4iia), a leading cause of catheter-associated urinary tract infections[61] relative to a common medical device material, PVC[62].

Figures 4ia and 4iia show that samples of GANPEG and LIG10K hydrogels soaked in deionized water for 7 days demonstrated significantly greater resistance to adherence of both pathogens relative to PVC controls after challenge periods up to 24 h. Figures S7 and S8 (see supporting information) show similar results for the unwashed and 24h soaked samples. The observed durability and retention of antibacterial properties after rinsing is important with regards to clinical application of the lignin-containing materials as medical device coating technologies, and the associated need for prevention of infection throughout the period of device implantation[63]. The antibacterial activity of GAN-based hydrogels has previously been reported[64,65]. To determine the antibacterial effect of the LIG component, bacterial adherence to the seven-day soaked LIG10K hydrogels was expressed relative to the GANPEG materials, and the significantly greater resistance to adherence of *S. aureus* and *P. mirabilis* of the LIG-containing hydrogels can be seen in Figures 4ib and 4iib.

While this is the first report of the antibacterial properties of GAN-LIG hydrogels, LIG has previously demonstrated promising antimicrobial activities towards cultures of Gram-positive bacteria and yeast[15,66]. With respect to the activity of LIG towards Gram-negative bacteria, mixed findings have been reported. No efficacy of LIG samples towards Gram-negative bacteria was reported in studies by Nada *et al.* and Dong *et al.* , whereas Yang *et al.* have recently demonstrated promising capacity of LIG-nanoparticle-containing nanocomposite films based on polyvinyl alcohol and chitosan in inhibiting the growth of two Gram-negative pathogens[15,67,68].

The encouraging resistance of the LIG-based hydrogels to adherence of the two pathogens observed herein offers promise for exciting new applications of this biomacromolecule in biomedical fields, where non-fouling materials and non-resistance-promoting antimicrobial strategies are urgently required. Moreover, due to the capability of sustaining drug release over several days, these materials can be loaded with antimicrobial compounds or other drugs to enhance their antimicrobial capabilities and deliver drugs to improve therapeutic outcomes.

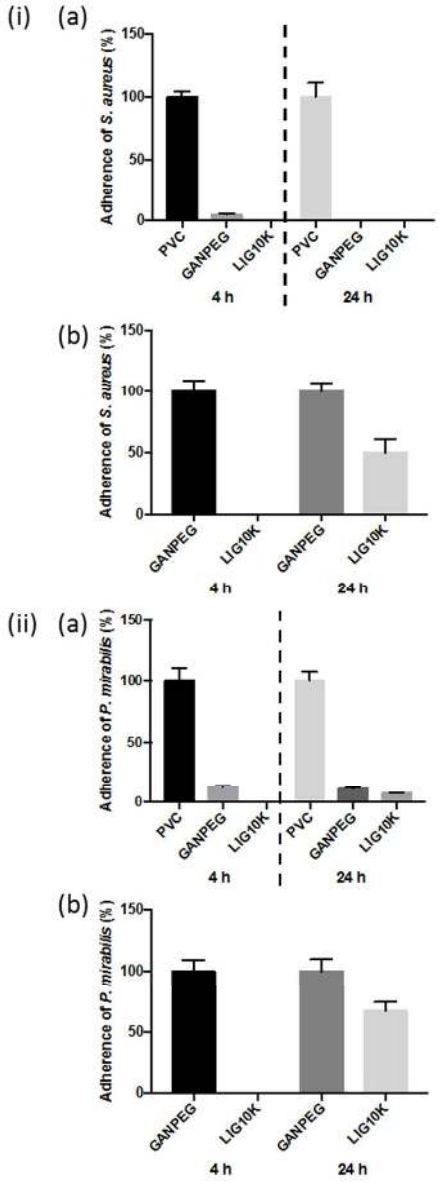

Figure 4. Adherence (%) of (i) *S. aureus* and (ii) *P. mirabilis* to surfaces of LIG10K pre-soaked in deionized water for seven days relative to (a) PVC and (b) GANPEG controls after 4 h and 24 h incubation at 37°C. Columns and error bars represent means ± standard deviations ($n \geq 5$).

3.5. Microwave-assisted crosslinking of LIG-based hydrogels

As previously mentioned, the developed process can be considered a green process due to the lack of toxicity of any of the solvents or by-products. Besides, the process is simple and can be performed in the solid state after combining the reagents. However, the crosslinking time is long and requires temperatures of 80°C over 24h. This is acceptable at the laboratory scale but would be a limiting

factor for industrial production. In order to obtain LIG-based hydrogels by a more efficient crosslinking process we explored the use of MW radiation.

The crosslinking process was ascertained with FTIR spectroscopy (Figure 5A). It can be seen that the GAN carbonyl peaks presented a shift due to the esterification reaction[45]. The peaks displayed higher shifts after the MW treatment than after the conventional oven treatment (Figure 1B). This suggests that the crosslinking process was more efficient since the hydrogels presented a higher degree of esterification after the 1 h treatment than after 24 h with the conventional process.

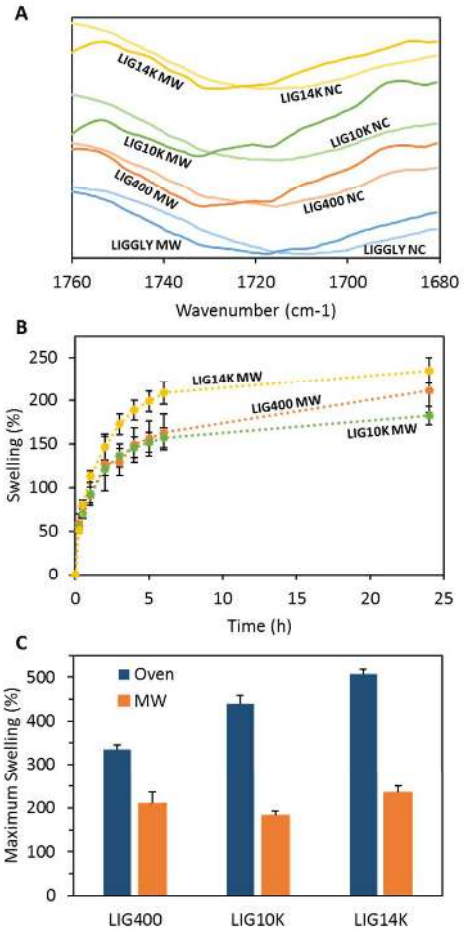

Figure 5. Carbonyl region of LIG/GAN/PEG hydrogels before (NC) and after the MW-assisted crosslinking process (A). Swelling kinetics in PBS of LIG-based hydrogels crosslinked using the MW-assisted process (B). Maximum swelling in PBS of LIG-based hydrogels crosslinked in the oven and in the microwave (C). (n=3).

The water uptake of the obtained hydrogels was evaluated (Figure 5B). LIGGLY hydrogels obtained from the MW assisted procedure were brittle and the swelling study could not be completed due to disintegration of the samples during the swelling process. It can be seen that the swelling profiles remained similar but the degree of swelling was significantly lower than for the hydrogels prepared using the conventional process. In order to compare the degree of swelling of the crosslinked materials prepared using both processes, Figure 5C shows the maximum swelling of all the formulations. It is obvious from this figure that the MW process yields hydrogels with higher crosslinking degrees due to the lower extent of swelling than for the oven crosslinked hydrogels ($p < 0.05$).

The mechanism behind the MW assisted crosslinking of the hydrogels is still unknown. We mentioned before that the OH and COOH groups should be aligned in the films before the crosslinking reaction. We hypothesize that the MW radiation provides a more efficient way of providing the energy required for the esterification reaction. Conventional ovens heat the material from the outside. On the other hand, microwave radiation penetrates into the materials providing volumetric heating[69], allowing a more efficient crosslinking reaction. Finally, MW heating is more efficient and likely to have higher temperatures than during the conventional process.

More experiments should be done to optimize MW-assisted crosslinking of LIG hydrogels. However, the promising results shown here suggest that the crosslinking process can be improved significantly. The MW process is shorter, more sustainable as it requires less energy than the thermal process[34] and overall, it will lead to the production of lower cost materials.

Conclusions

The present work describes a simple, green procedure to prepare LIG-based hydrogels. The process does not require the use of toxic solvents and one of the main components of the hydrogel is a renewable material. LIG hydrogels were successfully obtained after combination of the biomolecule with GAN, a polyacid, and PEG through an esterification reaction. It was demonstrated that the molecular weight of the PEG influenced hydrogel properties, including the final LIG content and water uptake capacity. The prepared hydrogels showed LIG contents ranging between 40% and 24% and water uptake capabilities up to 500%. The highest LIG contents and swelling capacities were obtained when PEGs with higher molecular weights of 14,000 and 10,000 were used. The prepared hydrogels were able to be loaded with hydrophobic compounds and to sustain the release for up to 4 days. Hydrogels obtained by using PEG with a molecular weight of 10,000 showed the best

properties in terms of drug loading and release. Additionally, the antimicrobial properties of LIG-based hydrogel materials crosslinked using PEG 10,000 were evaluated using two common pathogens responsible for medical device-associated infections, *S. aureus* and *P. mirabilis*. The results of these studies demonstrated that LIG-based hydrogels showed significant resistance to bacterial adherence when compared to PVC and similar hydrogels that do not contain LIG. Consequently, LIG-based hydrogels present promising properties as medical material coatings based on their resistance to infection and ability to release drugs over several days. Finally, we demonstrated that the hydrogel preparation can be accelerated by using MW radiation. In this way the crosslinking time was reduced from 24h to 1h by using the MW-assisted process, thereby lowering the energy consumption. This was a proof of concept and more work is needed to optimize the MW crosslinking step, however, these findings suggest that MW treatment can be used as an alternative way to obtain LIG-based hydrogels in an easier, lower cost and greener way.

Acknowledgements

The authors are thankful to Dr. D. Apperley for his assistance with ^{13}C-NMR experiments. This work was supported by the Wellcome Trust Biomedical Vacation Scholarship (207213/Z/17/Z and 207168/Z/17/Z) and the Royal Society Research Grant (RG170090).

Supporting Information

Supporting information contains pure lignin/hydrogel FTIR spectra, solid state ^{13}C-NMR and SEM images. Additionally, supporting information contains results obtained for curcumin release mathematical modelling and *in vitro* microbiological assessment results.

References

1. Kai, D.; Tan, M. J.; Chee, P. L.; Chua, Y. K.; Yap, Y. L.; Loh, X. J. Towards lignin-based functional materials in a sustainable world. *Green Chem.* **2016***, 18*, 1175-1200, DOI 10.1039/C5GC02616D.

2. Palm, M.; Zacchi, G. Separation of hemicellulosic oligomers from steam-treated spruce wood using gel filtration. *Sep. Purif. Technol.* **2004***, 36*, 191-201, DOI 10.1016/S1383-5866(03)00215-6.

3. Laurichesse, S.; Avérous, L. Chemical modification of lignins: Towards biobased polymers. *Prog. Polym. Sci.* **2014***, 39*, 1266-1290, DOI 10.1016/j.progpolymsci.2013.11.004.

4. Doherty, W. O. S.; Mousavioun, P.; Fellows, C. M. Value-adding to cellulosic ethanol: Lignin polymers. *Ind. Crop. Prod.* **2011***, 33*, 259-276, DOI 10.1016/j.indcrop.2010.10.022.5. Thakur, V. K.; Thakur, M. K.; Gupta, R. K. Graft copolymers from cellulose: Synthesis, characterization and evaluation. *Carbohydr. Polym.* **2013***, 97*, 18-25, DOI 10.1016/j.carbpol.2013.04.069.

6. Figueiredo, P.; Lintinen, K.; Hirvonen, J. T.; Kostiainen, M. A.; Santos, H. A. Properties and chemical modifications of lignin: Towards lignin-based nanomaterials for biomedical applications. *Prog. Mat. Sci.* **2018***, 93*, 233-269, DOI 10.1016/j.pmatsci.2017.12.001.

7. Thakur, V. K.; Thakur, M. K. Recent advances in green hydrogels from lignin: a review. *Int. J. Biol. Macromol.* **2015***, 72*, 834-847, DOI 10.1016/j.ijbiomac.2014.09.044.

8. Domínguez-Robles, J.; Espinosa, E.; Savy, D.; Rosal, A.; Rodríguez, A. Biorefinery Process Combining Specel® Process and Selective Lignin Precipitation using Mineral Acids. *Bioresources* **2016***, 11*, 7061-7077, DOI 10.15376/biores.11.3.7061-7077.

9. Sánchez, R.; Espinosa, E.; Domínguez-Robles, J.; Loaiza, J. M.; Rodríguez, A. Isolation and characterization of lignocellulose nanofibers from different wheat straw pulps. *Int. J. Biol. Macromol.* **2016***, 92*, 1025-1033, DOI 10.1016/j.ijbiomac.2016.08.019.

10. Liu, D.; Li, Y.; Qian, Y.; Xiao, Y.; Du, S.; Qiu, X. Synergistic Antioxidant Performance of Lignin and Quercetin Mixtures. *ACS Sustainable Chem. Eng.* **2017***, 5*, 8424-8428, DOI 10.1021/acssuschemeng.7b02282.

11. Kai, D.; Low, Z. W.; Liow, S.; Abdul Karim, A.; Ye, H.; Jin, G.; Li, K.; Loh, X. J. Development of Lignin Supramolecular Hydrogels with Mechanically Responsive and Self-Healing Properties. *ACS Sustainable Chem. Eng.* **2015***, 3*, 2160-2169, DOI 10.1021/acssuschemeng.5b00405.

12. Nandiwale, K. Y.; Danby, A. M.; Ramanathan, A.; Chaudhari, R. V.; Subramaniam, B. Zirconium-Incorporated Mesoporous Silicates Show Remarkable Lignin Depolymerization Activity. *ACS Sustainable Chem. Eng.* **2017***, 5*, 7155-7164, DOI 10.1021/acssuschemeng.7b01344.

13. Stewart, D. Lignin as a base material for materials applications: Chemistry, application and economics. *Ind. Crops Prod.* **2008***, 27*, 202-207, DOI 10.1016/j.indcrop.2007.07.008.

14. Pucciariello, R.; Bonini, C.; D'Auria, M.; Villani, V.; Giammarino, G.; Gorrasi, G. Polymer blends of steam-explosion lignin and poly(ε-caprolactone) by high-energy ball milling. *J. Appl. Polym. Sci.* **2008***, 109*, 309-313, DOI 10.1002/app.28097.

15. Dong, X.; Dong, M.; Lu, Y.; Turley, A.; Jin, T.; Wu, C. Antimicrobial and antioxidant activities of lignin from residue of corn stover to ethanol production. *Ind. Crops Prod.* **2011***, 34*, 1629-1634, DOI 10.1016/j.indcrop.2011.06.002.

16. Domínguez-Robles, J.; Sánchez, R.; Díaz-Carrasco, P.; Espinosa, E.; García-Domínguez, M. T.; Rodríguez, A. Isolation and characterization of lignins from wheat straw: Application as binder in lithium batteries. *Int. J. Biol. Macromol.* **2017***, 104*, 909-918, DOI 10.1016/j.ijbiomac.2017.07.015.

17. Azadfar, M.; Gao, A. H.; Bule, M. V.; Chen, S. Structural characterization of lignin: A potential source of antioxidants guaiacol and 4-vinylguaiacol. *Int. J. Biol. Macromol.* **2015***, 75*, 58-66, DOI 10.1016/j.ijbiomac.2014.12.049.

18. Kai, D.; Zhang, K.; Jiang, L.; Wong, H. Z.; Li, Z.; Zhang, Z.; Loh, X. J. Sustainable and Antioxidant Lignin-Polyester Copolymers and Nanofibers for Potential Healthcare Applications. *ACS Sustainable Chem. Eng.* **2017***, 5*, 6016-6025, DOI 10.1021/acssuschemeng.7b00850.

19. Thakur, S.; Govender, P. P.; Mamo, M. A.; Tamulevicius, S.; Mishra, Y. K.; Thakur, V. K. Progress in lignin hydrogels and nanocomposites for water purification: Future perspectives. *Vacuum* **2017***, 146*, 342-355, DOI 10.1016/j.vacuum.2017.08.011.

20. Domínguez-Robles, J.; Peresin, M. S.; Tamminen, T.; Rodríguez, A.; Larrañeta, E.; Jääskeläinen, A. S. Lignin-based hydrogels with "super-swelling" capacities for dye removal. *Int. J. Biol. Macromol.* **2018**, DOI 10.1016/j.ijbiomac.2018.04.044.

21. Caló, E.; Khutoryanskiy, V. V. Biomedical applications of hydrogels: A review of patents and commercial products. *Eur. Polym. J.* **2015***, 65*, 252-267, DOI 10.1016/j.eurpolymj.2014.11.024.

22. Peppas, N.; Hilt, J.; Khademhosseini, A.; Langer, R. Hydrogels in biology and medicine: From molecular principles to bionanotechnology. *Adv Mater* **2006***, 18*, 1345-1360, DOI 10.1002/adma.200501612.

23. Espinoza-Acosta, J., Torres-Chávez, P., Ramírez-Wong, B., López-Saiz, C., Montaño-Leyva,B. Antioxidant, Antimicrobial, and Antimutagenic Properties of Technical Lignins and Their Applications. *Bioresources* **2016***, 11*.

24. Wang, C.; Venditti, R. A. UV Cross-Linkable Lignin Thermoplastic Graft Copolymers. *ACS Sustainable Chem. Eng.* **2015***, 3*, 1839-1845, DOI 10.1021/acssuschemeng.5b00416.

25. Allsopp, A.; Misra, P. The constitution of the cambium, the new wood and the mature sapwood of the common ash, the common elm and the Scotch pine. *Biochem. J.* **1940***, 34*, 1078-1084.

26. Sarkanen, K. V.; Ludwig, C. H. *Lignins: Occurrence, formation, structure and reactions;* Wiley-Blackwell: New York, 1971; Vol. 10, pp 916, DOI 10.1002/pol.1972.110100315.

27. García-Domínguez, M. T.; García-Domínguez, J. C.; Feria, M. J.; Gómez-Lozano, D. M.; López, F.; Díaz, M. J. Furfural production from Eucalyptus globulus: Optimizing by using neural fuzzy models. *Chem. Eng. J.* **2013***, 221*, 185-192, DOI 10.1016/j.cej.2013.01.099.

28. Flory, P. J.; Rehner, J. J. Statistical Mechanics of Cross-Linked Polymer Networks I. Rubberlike Elasticity. *J. Chem. Phys.* **1943***, 11*, 512-520, DOI 10.1063/1.1723791.

29. Çaykara, T.; Kiper, S.; Demirel, G. Network parameters and volume phase transition behavior of poly(N-isopropylacrylamide) hydrogels. *J. Appl. Polym. Sci.* **2006***, 101*, 1756-1762, DOI 10.1002/app.23513.

30. Raj Singh, T. R.; McCarron, P. A.; Woolfson, A. D.; Donnelly, R. F. Investigation of swelling and network parameters of poly(ethylene glycol)-crosslinked poly(methyl vinyl ether-co-maleic acid) hydrogels. *Eur. Polym. J.* **2009***, 45*, 1239-1249, DOI 10.1016/j.eurpolymj.2008.12.019.

31. Bajpai, S. K.; Singh, S. Analysis of swelling behavior of poly(methacrylamide-co-methacrylic acid) hydrogels and effect of synthesis conditions on water uptake. *React. Funct. Polym.* **2006***, 66*, 431-440, DOI 10.1016/j.reactfunctpolym.2005.09.003.

32. Ritger, P. L.; Peppas, N. A simple equation for description of solute release I. Fickian and Non-Fickian release from non-swellable devices in the form of slabs, spheres, cylinders or discs. *J. Controlled Release* **1987***, 5*, 23-36, DOI 10.1016/0168-3659(87)90034-4.

33. Costa, P.; Manuel, J.; Lobo, S.; Sousa Lobo, J. M. Modeling and comparison of dissolution profiles. *European journal of pharmaceutical sciences* **2001***, 13*, 123-33, DOI 10.1016/S0928-0987(01)00095-1.

34. Larrañeta, E.; Lutton, R. E. M.; Brady, A. J.; Vicente-Pérez, E. M.; Woolfson, A. D.; Thakur, R. R. S.; Donnelly, R. F. Microwave-Assisted Preparation of Hydrogel-Forming Microneedle Arrays for Transdermal Drug Delivery Applications. *Macromol. Mater. Eng.* **2015***, 300*, 586-595, DOI 10.1002/mame.201500016.

35. Donnelly, R. F.; Singh, T. R. R.; Garland, M. J.; Migalska, K.; Majithiya, R.; McCrudden, C. M.; Kole, P. L.; Mahmood, T. M. T.; McCarthy, H. O.; Woolfson, A. D. Hydrogel-Forming Microneedle Arrays for Enhanced Transdermal Drug Delivery. *Adv. Funct. Mater.* **2012***, 22*, 4879-4890, DOI 10.1002/adfm.201200864.

36. Larrañeta, E.; Henry, M.; Irwin, N. J.; Trotter, J.; Perminova, A. A.; Donnelly, R. F. Synthesis and characterization of hyaluronic acid hydrogels crosslinked using a solvent-free process for potential biomedical applications. *Carbohydr. Polym.* **2018***, 181*, 1194-1205, DOI 10.1016/j.carbpol.2017.12.015.

37. Miles, A. A.; Misra, S. S.; Irwin, J. O. The estimation of the bactericidal power of the blood. *J. Hyg.* **1938***, 38*, 732-749.

38. Ripolin, A.; Quinn, J.; Larrañeta, E.; Vicente-Perez, E. M.; Barry, J.; Donnelly, R. F. Successful application of large microneedle patches by human volunteers. *Int. J. Pharm.* **2017***, 521*, 92-101, DOI 10.1016/j.ijpharm.2017.02.011.

39. Donnelly, R. F.; McCrudden, M. T. C.; Zaid Alkilani, A.; Larrañeta, E.; McAlister, E.; Courtenay, A. J.; Kearney, M.; Singh, T. R. R.; McCarthy, H. O.; Kett, V. L.; Caffarel-Salvador, E.; Al-Zahrani, S.; Woolfson, A. D. Hydrogel-Forming Microneedles Prepared from "Super Swelling" Polymers Combined with Lyophilised Wafers for Transdermal Drug Delivery. *PLoS ONE* **2014***, 9*, e111547, DOI 10.1371/journal.pone.0111547.

40. Vinardell, P. M.; Mitjans, M. Lignins and Their Derivatives with Beneficial Effects on Human Health. *Int. J. Mol. Sci.* **2017***, 18*, DOI 10.3390/ijms18061219.

41. Ojer, P.; Neutsch, L.; Gabor, F.; Irache, J. M.; López de Cerain, A. Cytotoxicity and cell interaction studies of bioadhesive poly(anhydride) nanoparticles for oral antigen/drug delivery. *J. Biomed. Nanotechnol.* **2013***, 9*, 1891-1903, DOI 10.1166/jbn.2013.1695.

42. Singh, T. R. R.; McCarron, P. A.; Woolfson, A. D.; Donnelly, R. F. Physicochemical characterization of poly(ethylene glycol) plasticized poly(methyl vinyl ether-co-maleic acid) films. *J Appl Polym Sci* **2009***, 112*, 2792, DOI 10.1002/app.29523.

43. Deepa, A. K.; Dhepe, P. L. Lignin Depolymerization into Aromatic Monomers over Solid Acid Catalysts. *ACS Catal.* **2015***, 5*, 365-379, DOI 10.1021/cs501371q.

44. Deepa, A. K.; Dhepe, P. L. Solid acid catalyzed depolymerization of lignin into value added aromatic monomers. *RSC Adv.* **2014**, *4*, 12625-12629, DOI 10.1039/C3RA47818A.

45. Sclavons, M.; Franquinet, P.; Carlier, V.; Verfaillie, G.; Fallais, I.; Legras, R.; Laurent, M.; Thyrion, F. C. Quantification of the maleic anhydride grafted onto polypropylene by chemical and viscosimetric titrations, and FTIR spectroscopy. *Polymer* **2000**, *41*, 1989-1999, DOI 10.1016/S0032-3861(99)00377-8.

46. Donnelly, R. F.; Morrow, D. I.; McCrudden, M. T.; Alkilani, A. Z.; Vicente-Pérez, E. M.; O'Mahony, C.; González-Vázquez, P.; McCarron, P. A.; Woolfson, A. D. Hydrogel-forming and dissolving microneedles for enhanced delivery of photosensitizers and precursors. *Photochem. Photobiol.* **2014**, *90*, 641-647, DOI 10.1111/php.12209.

47. Calo, E.; Barros, J. M. S. d.; Fernandez-Gutierrez, M.; San Roman, J.; Ballamy, L.; Khutoryanskiy, V. V. Antimicrobial hydrogels based on autoclaved poly(vinyl alcohol) and poly(methyl vinyl ether-alt-maleic anhydride) mixtures for wound care applications. *RSC Adv.* **2016**, *6*, 55211-55219, DOI 10.1039/C6RA08234C.

48. Lutton, R. E. M.; Larrañeta, E.; Kearney, M. C.; Boyd, P.; Woolfson, A. D.; Donnelly, R. F. A novel scalable manufacturing process for the production of hydrogel-forming microneedle arrays. *Int. J. Pharm.* **2015**, *494*, 417-429, DOI 10.1016/j.ijpharm.2015.08.049.

49. Calo, E.; Barros, J.; Ballamy, L.; Khutoryanskiy, V. V. Poly(vinyl alcohol)-Gantrez® AN cryogels for wound care applications. *RSC Adv.* **2016**, *6*, 105487-105494, DOI 10.1039/C6RA24573K.

50. Moreno, E.; Schwartz, J.; Larrañeta, E.; Nguewa, P. A.; Sanmartín, C.; Agüeros, M.; Irache, J. M.; Espuelas, S. Thermosensitive hydrogels of poly(methyl vinyl ether-co-maleic anhydride) - Pluronic(®) F127 copolymers for controlled protein release. *Int. J. Pharm.* **2014**, *459*, 1-9, DOI 10.1016/j.ijpharm.2013.11.030.

51. Larraneta, E.; Barturen, L.; Ervine, M.; Donnelly, R. F. Hydrogels based on poly(methyl vinyl ether-co-maleic acid) and Tween 85 for sustained delivery of hydrophobic drugs. *Int. J. Pharm.* **2018**, *538*, 147-158, DOI 10.1016/j.ijpharm.2018.01.025.

52. Capello, C.; Fischer, U.; Hungerbuhler, K. What is a green solvent? A comprehensive framework for the environmental assessment of solvents. *Green Chem.* **2007**, 927-934, DOI 10.1039/B617536H.

53. Larrañeta, E.; Stewart, S.; Ervine, M.; Al-Kasasbeh, R.; Donnelly, R. F. Hydrogels for Hydrophobic Drug Delivery. Classification, Synthesis and Applications. *Journal of Functional Biomaterials* **2018**, *9*, DOI 10.3390/jfb9010013.

54. Gupta, S. C.; Prasad, S.; Kim, J. H.; Patchva, S.; Webb, L. J.; Priyadarsini, I. K.; Aggarwal, B. B. Multitargeting by curcumin as revealed by molecular interaction studies. *Nat. Prod. Rep.* **2011**, *28*, 1937-1955, DOI 10.1039/c1np00051a.

55. Mohan, P. R. K.; Sreelakshmi, G.; Muraleedharan, C. V.; Joseph, R. Water soluble complexes of curcumin with cyclodextrins: Characterization by FT-Raman spectroscopy. *Vib. Spectrosc.* **2012**, *62*, 77-84, DOI 10.1016/j.vibspec.2012.05.002.

56. Weber, D. J.; Anderson, D.; Rutala, W. A. The role of the surface environment in healthcare-associated infections. *Curr. Opin. Infect. Dis.* **2013***, 26*, DOI 10.1097/QCO.0b013e3283630f04.

57. Hall, C. W.; Mah, T. F. Molecular mechanisms of biofilm-based antibiotic resistance and tolerance in pathogenic bacteria. *FEMS Microbiol. Rev.* **2017***, 41*, 276-301, DOI 10.1093/femsre/fux010.

58. Irwin, N. J.; McCoy, C. P.; Jones, D. S.; Gorman, S. P. Infection-Responsive Drug Delivery from Urinary Biomaterials Controlled by a Novel Kinetic and Thermodynamic Approach. *Pharm. Res.* **2013***, 30*, 857-865, DOI 10.1007/s11095-012-0927-x.

59. Shi, H.; Liu, H.; Luan, S.; Shi, D.; Yan, S.; Liu, C.; Li, R. K. Y.; Yin, J. Effect of polyethylene glycol on the antibacterial properties of polyurethane/carbon nanotube electrospun nanofibers. *RSC Adv.* **2016***, 6*, 19238-19244, DOI 10.1039/C6RA00363J.

60. Tong, S. Y. C.; Davis, J. S.; Eichenberger, E.; Holland, T. L.; Fowler, V. G. Staphylococcus aureus Infections: Epidemiology, Pathophysiology, Clinical Manifestations, and Management. *Clin. Microbiol. Rev.* **2015***, 28*, 603-661, DOI 10.1128/CMR.00134-14.

61. Norsworthy, A. N.; Pearson, M. M. From Catheter to Kidney Stone: The Uropathogenic Lifestyle of *Proteus mirabilis*. *Trends Microbiol.* **2017***, 25*, 304-315, DOI 10.1016/j.tim.2016.11.015.

62. McKeen, L. W. 3 - Plastics Used in Medical Devices. In *Handbook of Polymer Applications in Medicine and Medical Devices*; Modjarrad, K., Ebnesajjad, S., Eds.; William Andrew Publishing: Oxford, 2014; pp 21-53, DOI 10.1016/B978-0-323-22805-3.00003-7.

63. Cheng, H.; Li, Y.; Huo, K.; Gao, B.; Xiong, W. Long-lasting in vivo and in vitro antibacterial ability of nanostructured titania coating incorporated with silver nanoparticles. *Journal of Biomedical Materials Research Part A* **2014***, 102*, 3488-3499, DOI 10.1002/jbm.a.35019.

64. Nudera, W. J.; Fayad, M. I.; Johnson, B. R.; Zhu, M.; Wenckus, C. S.; BeGole, E. A.; Wu, C. D. Antimicrobial Effect of Triclosan and Triclosan with Gantrez on Five Common Endodontic Pathogens. *J Endod.* **2007***, 33*, 1239-1242, DOI 10.1016/j.joen.2007.06.009.

65. Boehm, R. D.; Miller, P. R.; Singh, R.; Shah, A.; Stafslien, S.; Daniels, J.; Narayan, R. J. Indirect rapid prototyping of antibacterial acid anhydride copolymer microneedles. *Biofabrication* **2012***, 4*, 011002, DOI 10.1088/1758-5082/4/1/011002.

66. Gabov, K.; Oja, T.; Deguchi, T.; Fallarero, A.; Fardim, P. Preparation, characterization and antimicrobial application of hybrid cellulose-lignin beads. *Cellulose* **2017***, 24*, 641-658, DOI 10.1007/s10570-016-1172-y.

67. Yang, W.; Owczarek, J. S.; Fortunati, E.; Kozanecki, M.; Mazzaglia, A.; Balestra, G. M.; Kenny, J. M.; Torre, L.; Puglia, D. Antioxidant and antibacterial lignin nanoparticles in polyvinyl alcohol/chitosan films for active packaging. *Ind. Crops Prod.* **2016***, 94*, 800-811, DOI 10.1016/j.indcrop.2016.09.061.

68. Nada, A. M. A.; El-Diwany, A. I.; Elshafei, A. M. Infrared and antimicrobial studies on different lignins. *Acta Biotechnol.* **1989***, 9*, 295-298, DOI 10.1002/abio.370090322.

69. Sun, J.; Wang, W.; Yue, Q. Review on Microwave-Matter Interaction Fundamentals and Efficient Microwave-Associated Heating Strategies. *Materials* **2016***, 9*, DOI 10.3390/ma9040231.

For Table of Contents Use Only

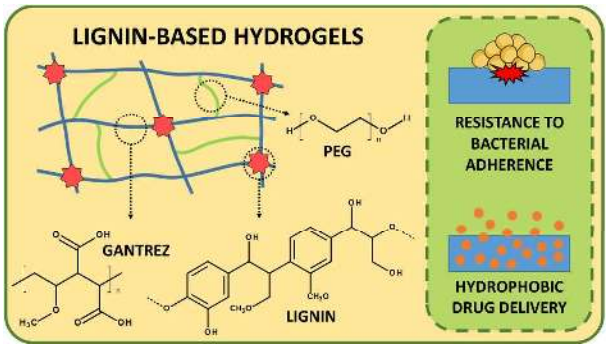

Synopsis: Lignin-based hydrogels were synthesized using a green-process. The resulting hydrogels showed hydrophobic drug delivery capabilities and resistance to bacterial adherence.